Desalination 271 (2011) 72–79

Contents lists available at ScienceDirect

Desalination

journal homepage: www.elsevier.com/locate/desal

A solar-powered reverse osmosis system for high recovery of freshwater from saline groundwater

P.A. Davies *

Sustainable Environment Research Group, School of Engineering and Applied Science, Aston University, Birmingham B4 7ET, UK

ARTICLE INFO

Article history:
Received 30 July 2010
Received in revised form 4 December 2010
Accepted 6 December 2010
Available online 8 January 2011

Keywords:
Solar
Rankine cycle
Reverse osmosis
Batch mode
Brackish water

ABSTRACT

Desalination of groundwater is essential in arid regions that are remote from both seawater and freshwater resources. Desirable features of a groundwater desalination system include a high recovery ratio, operation from a sustainable energy source such as solar, and high water output per unit of energy and land. Here we propose a new system that uses a solar-Rankine cycle to drive reverse osmosis (RO). The working fluid such as steam is expanded against a power piston that actuates a pump piston which in turn pressurises the saline water thus passing it through RO membranes. A reciprocating crank mechanism is used to equalise the forces between the two pistons. The choice of batch mode in preference to continuous flow permits maximum energy recovery and minimal concentration polarisation in the vicinity of the RO membrane. This study analyses the sizing and efficiency of the crank mechanism, quantifies energy losses in the RO separation and predicts the overall performance. For example, a system using a field of linear Fresnel collectors occupying 1000 m^2 of land and raising steam at 200 °C and 15.5 bar could desalinate 350 m^3/day from saline water containing 5000 ppm of sodium chloride with a recovery ratio of 0.7.

Symbol	Units	Description
A	m^2	Area of RO membrane
b	m	Height of reverse osmosis channel
B	ms^{-1}	Salt transport coefficient of membrane
C		Concentration polarisation modulus
D	m^2s^{-1}	Diffusion coefficient of salt
E	J	Energy of desalination
F	N	Force of pistons
J	ms^{-1}	Flux of water permeating the membrane
k		Ratio of pressure from pump divided by osmotic pressure
l	m	Length of RO channel
n		Index of polytropic expansion
p	Pa	Pressure
Q	m^3s^{-1}	Flow
r		Recovery ratio (permeate flow divided by feed flow)
R	m	Crank radius
S	ms^{-1} Pa^{-1}	Permeability of membrane
V	m^3	Volume
x	m	Displacement of power piston
y	m	Displacement of pump piston
α,β,ε		Dimensionless parameters used in analysis of crank motion
η		Efficiency
μ	Pa s	Viscosity
θ		Crank angle

Symbol	Units	Description
Subscripts		
1		Initial position
2		Final position
coll		of collector
circ		of recirculation loop
crank		of crank
osm		osmotic
osmf		osmotic, of feed
osmp		osmotic, of permeate
rank		of Rankine cycle
RO		of RO separation
x		of power piston
y		of pump piston
Abbreviations		
LFR		Linear Fresnel reflector
PTC		Parabolic trough collector
RO		Reverse osmosis

1. Introduction

Salinity of soil and groundwater is a widespread problem occurring across all inhabited continents [1]. Significant areas of land lie above brackish groundwater, especially in the world's arid and semi-arid regions. In the absence of rain, desalination of groundwater may be the only way to provide freshwater for inland

* Tel.: +44 121 204 3724; fax: +44 121 204 3683.
E-mail address: p.a.davies@aston.ac.uk.

0011-9164 © 2010 Elsevier B.V. Open access under CC BY-NC-ND license.
doi:10.1016/j.desal.2010.12.010

regions. Examples of countries where groundwater desalination systems are already used include Australia, Egypt, India, Israel, Jordan, Morocco, the United Arab Emirates and the United States.

As with seawater, the desalination of groundwater requires energy which is typically supplied from fossil fuel sources. The need to satisfy the growing demand for water, while reducing the environmental impact associated with the use of such energy, makes it important to improve the efficiency of the desalination process and to take greater advantage of renewable energies such as solar.

Many solar-driven desalination technologies have been studied and several have been implemented [2]. Most fall into one of two categories: (i) thermal distillation processes or (ii) non-thermal membrane separation processes such as electro-dialysis and reverse osmosis (RO). In the first category, single effect solar stills can provide just a few litres of water per square metre of captured sunlight per day while multiple effect solar stills may provide tens of litres per square metre [3].

Reverse osmosis is generally considered the most energy efficient method of desalination. It requires mechanical work, rather than heat, as input. Most of the solar-RO plants that have been built to date use photovoltaic (PV) arrays to provide this work [4]. For example, Richards et al. [5] have reported trials in Australia with a system producing about 0.5 m^3/day of freshwater from groundwater at a salinity of 3000 ppm, using a 0.26 kWp generator occupying an area of 2 m^2. This corresponds to 250 l/m^2 per day, which is an order of magnitude above that readily achievable with solar stills. Such technology based on PV is reliable and simple to implement, but does not benefit from significant economies or efficiencies of scale. Consequently, the largest system reported gave an output of only 76 m^3 per day [4,6]. In contrast, desalination plants powered by conventional fuels exist with outputs above 100 000 m^3 per day.

In place of PV, solar-thermal power plant may be used to generate the work needed to drive the RO process. So far, however, very few such plants have been constructed. Notably, the one constructed at El Hamrawin in Egypt in 1981 reportedly produced 130 l per day per m^2 of solar collector, when fed with brackish water of salinity 3000 ppm [7]. This plant used the Rankine cycle, with Freon-11 as the working fluid. Freon-11 is an ozone depleting substance now banned under the Montreal Protocol. More recently, García-Rodriguez and Delgado-Torres have presented calculations for Rankine cycle–RO systems using a variety of alternative working fluids [8]. They predict specific solar energy consumptions ranging from 32 to 95 MJ/m^3 (8.9 to 26 kWh/m^3) which, based on a useful irradiation of 5 kWh/m^2 per day (18 MJ/m^2 per day) would give water outputs per collector area of 190 to 560 l/m^2 per day. Some of the working fluids they consider, such as benzene and toluene, are toxic while others such as siloxanes are more benign but less readily available. The schematic of the typical solar-Rankine–RO system studied by those authors is reproduced in Fig. 1.

Most solar-thermal power plants in use today, such as the ones located in California's Mojave Desert, are based on the steam Rankine cycle and generate electricity which is fed to the grid. The possibility of coupling to desalination equipment has been studied and could be implemented in the future [9]. In contrast to PV, however, steam power plant is more efficient and economical at large scales, typically >10 MW electrical output, which if used for desalination by RO would result in water outputs of 10 000 m^3/day or more. Despite the growth of interest in solar-powered desalination, there is still a lack of proven and viable solutions at the intermediate scale of roughly 50 to 5000 m^3/day. For groundwater sources in particular, such scales are needed since, unlike the sea, individual wells and aquifers have limited capacity to feed desalination plants.

Groundwater is typically less saline than seawater. On this account, the energy requirement for desalination by RO is lower. On the other hand, desalination of groundwater is preferably operated at high recovery ratio. This is to avoid wasting precious groundwater and to minimise the volume of concentrated brine rejected, the disposal of which poses an environmental problem. High recovery tends to require high energy inputs thus partially offsetting the energy saving from the lower feed salinity. This trade off is illustrated by the following standard equation for the thermodynamic minimum energy E required to recover a volume V of freshwater from saline feed water having an osmotic pressure of P_{osmf} at a recovery ratio r.

$$E = Vp_{osmf}\frac{1}{r}ln\frac{1}{(1-r)} \quad (1)$$

Following this brief discussion, we could propose the following ideal requirements of a solar-powered RO system for brackish groundwater:

- Low specific solar energy consumption and thus high water output per area of solar collector and of land occupied
- High recovery ratio
- Avoidance of toxic, environmentally harmful or scarcely available working fluids (water or air are ideal fluids in this respect)
- Use of commonly available materials, components and manufacturing processes thus favouring low cost and good availability
- Viability at the intermediate scale of 50 to 5000 m^3 water output.

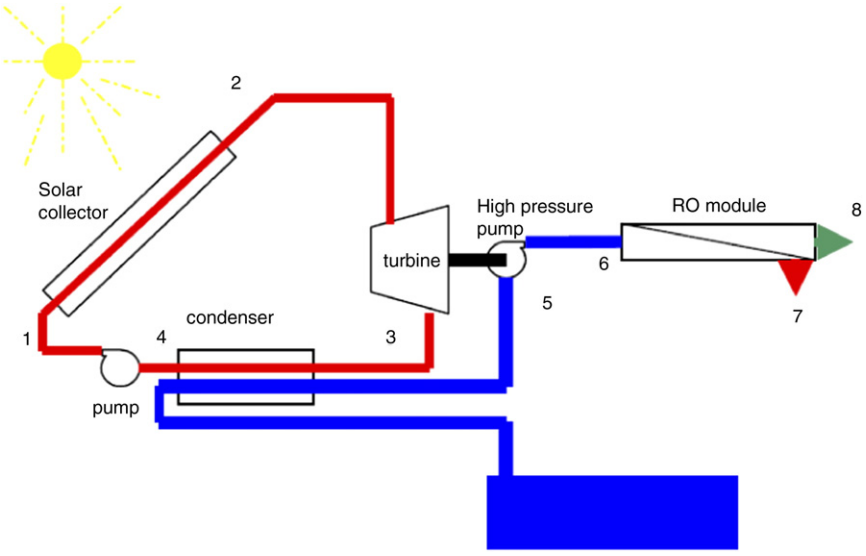

Fig. 1. Schematic of a conventional solar-powered RO system based on the Rankine cycle (reproduced from [8] with permission).

With the aim of meeting these requirements, this paper puts forward a new concept of solar-powered RO based on the steam Rankine cycle. The specific objective is to analyse the concept to find the efficiency and output in relation to the design and operating parameters. Examples of system designs will be outlined. Note that no experiment has yet been carried out, but it is intended that this analysis will inform future experimentation and development.

First the rationale and concept of the design will be explained with reference to the shortcomings of the existing approaches that use the Rankine cycle.

2. Existing approaches coupling the Rankine cycle to RO

A principal drawback in using the steam Rankine cycle at smaller scales (e.g. <1 MW shaft output) is the inefficiency of small steam turbines, which results from blade friction loss and leakage loss [10]. To avoid these losses, the steam may be expanded using a piston instead of a turbine. Once this approach is adopted, it is logical to omit the step of converting the linear motion of the steam power piston to continuous rotary motion of the pump. Instead, a so-called steam pump may be used, in which the steam power piston is coupled directly to the piston of a reciprocating pump. Standard designs of steam pump are described, for example, in reference [11]. However, a difficulty with steam pumps is that the force provided by the power piston varies as the piston moves through its cycle. To overcome this problem, Childs et al. have described a hydraulic unit to add to or subtract from the power output and thus compensate for such cyclic variations in force [12]. This paper sets out a simpler method, in which the problem of varying forces is overcome by mechanical means.

Another feature of the concept proposed here is the ability to drive a batch-wise RO process, which is in principle the most energy-efficient way of operating RO. The advantage of the batch-wise operation over the more common continuous flow operation can be explained in terms of the concentrations of salt in the liquid at different positions in the RO module of Fig. 1. As the saline water passes through the module, water is removed and the increased concentration leads to increased osmotic pressure at the outlet, hence increasing the energy needed for the process. In the batch process, however, concentration is kept almost uniform through the system at each moment in time and wastage of energy due to concentration gradients inside the system is therefore minimised.

3. The concept

Fig. 2 illustrates the essence of the new concept. The steam (or other working fluid) is supplied from solar collectors to an expansion cylinder and expands against a piston (referred to as the power piston). This piston drives a second piston (referred to as the pump piston) which is used to pressurise saline water against the semi-permeable membrane that allows freshwater to pass while retaining the salt. To prevent accumulation of salts near the surface of the membrane (ie. concentration polarisation) a means of stirring the solution near the membrane is included.

As the steam expands, its pressure will decrease, according to the well-known polytropic expression:

$$p_x V_x^n = constant_1 \tag{2}$$

where n is a constant typically having a value of 1.135 for wet steam and 1.3 for superheated steam [10]. As water is expelled from the saline solution, the concentration of salt will increase and thus will the osmotic pressure according to the van't Hoff type relation (it is assumed that virtually all the salt is retained by the membrane and that concentrations are low enough for this relation to apply):

$$p_{osm} V_y = constant_2 \tag{3}$$

Consequently, as the two pistons in Fig. 2 move to the right, the force F_x available from the power piston *decreases* while the force F_y needed to move the pump piston *increases*. This illustrates why a direct coupling of the two pistons, as used in a conventional steam pump, will not be satisfactory. Instead, a mechanism (indicated schematically in Fig. 2) is needed to provide an increasing mechanical advantage as the pistons move. This can be achieved in practice by the arrangement shown in Fig. 3 that uses a crank (OP) and linkages (LP and MP) to couple the two pistons. From the equilibrium of moments on the crank, it is evident that (with the assumption that the linkages are substantially longer than the crank radius) the mechanical advantage of the system when the crank is at an angle θ to the horizontal is approximately:

$$F_y / F_x = \tan\theta \tag{4}$$

Therefore the mechanical advantage increases as the crank rotates anti-clockwise and θ increases. For example, $\theta = 10°$ gives a mechanical advantage of 0.176 increasing 32-fold to 5.67 at $\theta = 80°$. Note that, unlike in conventional piston engines and pumps using crankshafts, the crank does not rotate through a full circle; it rotates through less than 90° and changes direction in order to restore the system to its original position. The precise angular positions of the reciprocating crank at the beginning and end of the cycle are carefully chosen to optimise the efficiency of the system but typically have values of about $\theta_1 = 10°$ and $\theta_2 = 80°$ respectively.

Fig. 3 shows also the more practical arrangement corresponding to the stirrer in Fig. 2. The function of the stirrer is performed by a recirculation pump and a membrane module of standard, spiral wound construction. The rapid re-circulating flow sweeps away salts accumulating near the surface of the membrane. Note that the energy needed to

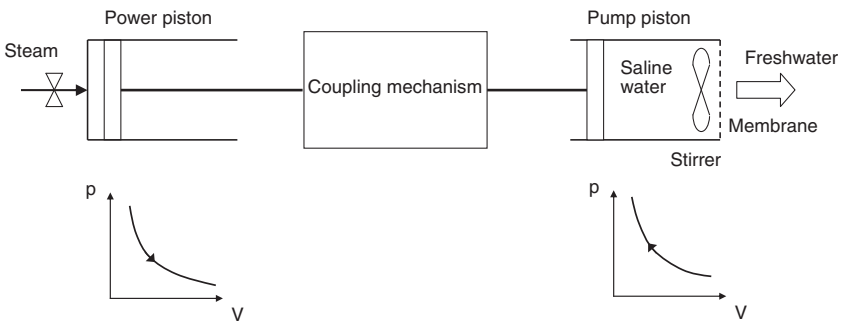

Fig. 2. Essential features of the proposed new concept. A power piston drives the pump piston via a coupling mechanism. The pump piston pressurises saline water against the semi-permeable membrane. The notional stirrer reduces concentration polarisation near the membrane. As the power piston advances to the right, the driving force available diminishes, while that needed for the reverse osmosis process increases. (This is illustrated by the two p–V graphs). To match these forces, the coupling mechanism must provide a gradually increasing mechanical advantage.

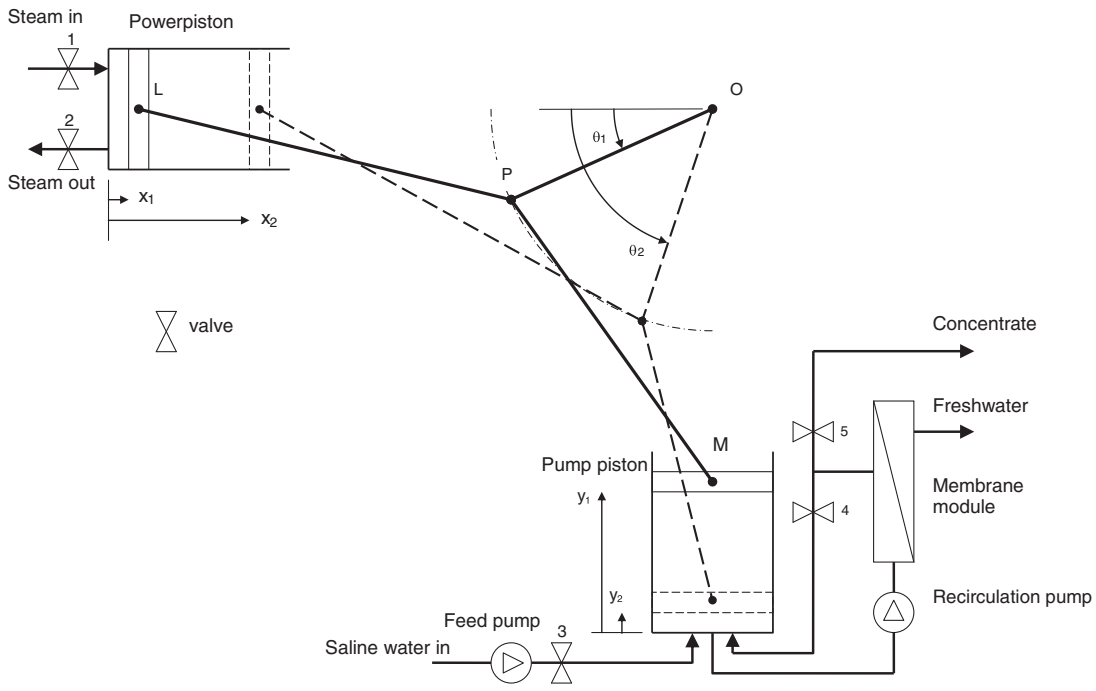

Fig. 3. Practical realisation of the concept. The coupling mechanism of Fig. 2 is realised as an arrangement of crank and linkages, in which the crank OP reciprocates about the fixed point O. This arrangement provides increasing mechanical advantage as the power piston advances. The pump piston pressurises batches of saline water that are recirculated through the membrane by the recirculation pump. The initial and final positions of the system are shown by bold and dashed lines respectively.

drive the recirculation pump is small compared to the energy needed for the whole system, because this pump is working against a low pressure as needed to move the water tangentially to the membrane, which is small compared to the osmotic pressure of the fluid.

When the pump piston reaches the end of its travel, it is necessary to purge the RO module and pump cylinder of the concentrated salt solution. This is done by opening the valves 3 and 5, while closing valve 4 (refer to Fig. 3 for valve numbering), and introducing the feed solution to wash out the system. Then valve 5 is closed again, such that the feed solution causes the pump piston to move upward, returning the whole system to its original position. Table 1 summarises the sequence of operation which is described conveniently in terms of the approximate values of the crank angle θ.

4. Analysis

The analysis focuses on the calculation of losses that will cause the output to be less than that indicated by Eq. (1). For example, though the crank mechanism will improve the matching of forces between the two pistons, it is not guaranteed that the crank motion is the ideal one needed for maximum efficiency: there may be some energy losses from any remaining mismatch. Further losses occur in the RO system itself. All these losses will be estimated in this section, following which water outputs for the whole system including solar collector will be estimated. Note that certain losses such as friction in the crank mechanism are not taken into account, as these are not intrinsic to the concept and could be minimised by careful design.

4.1. The crank mechanism

The starting point for this analysis is provided by Eqs. (2) and (3). With regard to Eq. (3), however, it is important to take into account the fact that the pressure acting on the piston will be somewhat larger than the osmotic pressure, due to the effects of concentration polarisation and the resistance to flow of water through the membrane. This increase will be represented by the constant overpressure factor k ($k>1$, to be discussed further in the next section) such that $P_y = kP_{osm}$ and Eq. (3) is then rewritten:

$$p_y V_y = constant_3 \tag{5}$$

For each of Eqs. (2) and (5), integration under the pV curve yields the amount of work transferred. Over any interval of time, the work done by the power piston should equal that absorbed by the pump piston. Since the volume of each of the cylinders is proportional to the linear displacements x and y of the respective piston measured from the end of the cylinder to the face of the piston:

$$p_{x1}V_{x1}\left[\frac{1-\left(\frac{x_1}{x}\right)^{n-1}}{n-1}\right] = p_{y1}V_{y1}ln\left[\frac{y_1}{y}\right] \tag{6}$$

where the subscript 1 indicates the initial state of the system at the beginning of the power stroke. Following again the simplifying assumption that the lengths of the linkages LP and MP in Fig. 3 are significantly longer than the radius of the crank, the x and y

Table 1
Sequence of operation of the desalination machine shown in Fig. 3.

	Process stage		Valves					Pumps	
Crank angle θ approx.	Expansion cylinder	Pump cylinder	1	2	3	4	5	Feed	Re-circulation
10–20°	Admit steam	Pump water through membrane	Open	Closed	Closed	Open	Closed	Off	On
20–80°	Expand steam	Ditto	Closed	Closed	Closed	Open	Closed	Off	On
80°	At rest	Purging	Closed	Open	Open	Closed	Open	On	On
80–10°	Exhaust steam	Refill	Closed	Open	Open	Closed	Closed	On	Off

displacements of the pivot point P are approximately equal to those of the power and pump piston respectively. In this case, Eq. (6) defines the ideal locus of the pivot point P.

However, this ideal locus cannot be achieved in practice, because the crank provides circular motion, whereas Eq. (6) describes an arc which is not perfectly circular. Thus the task is to choose a circular path that approximates Eq. (6). To achieve this, the following variables may be chosen: the radius R of the crank, its initial and final angular positions θ_1 and θ_2, and the strokes Δx and Δy of the pump and power piston respectively.

The analysis used here chooses the geometry of the crank such that: (i) the initial and final positions of the point P match those of Eq. (6), and (ii) the initial and final gradients (dy/dx) of the motion of P and therefore the mechanical advantage also match initially and finally. Based on these criteria of matching, the analysis (the details of which are given in Appendix A) yields the following expressions which, for maximum generality, are given as dimensionless ratios thus allowing a very wide range of designs and sizes to be analysed.

For the stroke Δy of the pump piston relative to that Δx of the power piston

$$\frac{\Delta y}{\Delta x} = \sqrt{\frac{2-\beta(1+\varepsilon)}{\beta[(2\beta-1)\varepsilon-1]}} \tag{7}$$

Where the dimensionless quantities β and ε are defined by:

$$\beta = \frac{\alpha}{r}\left[\left(\frac{p_{x1}}{p_{x2}}\right)^{1/n} - 1\right] \tag{8}$$

$$\varepsilon = \frac{(1-r)}{(p_{x1}/p_{x2})} \tag{9}$$

and

$$\alpha = \frac{p_{x1}V_{x1}}{p_{y1}V_{y1}} = \frac{(n-1)ln\left[\frac{1}{(1-r)}\right]}{\left[1-\left(\frac{p_{x1}}{p_{x1}}\right)^{\frac{n-1}{1}}\right]} \tag{10}$$

Note that ε represents the ratio of the initial mechanical advantage of the mechanism to the final one and in practice its value is much less than 1. The radius R of the crank is calculated by simple trigonometry to be:

$$\frac{R}{\Delta x} = \frac{\sqrt{1+\left(\frac{\Delta y}{\Delta x}\right)^2}}{2\sin\left(\frac{\Delta\theta}{2}\right)} \tag{11}$$

whe re $\Delta\theta$ is the swept angle of the crank $\Delta\theta = \theta_2 - \theta_1$ and these initial and final angles are given by:

$$\theta_1 = \tan^{-1}\left[\frac{1}{\beta(\Delta y/\Delta x)}\right] \tag{12}$$

and

$$\theta_2 = \tan^{-1}\left[\frac{1}{\varepsilon\beta(\Delta y/\Delta x)}\right] \tag{13}$$

The three input parameters to the foregoing equations are the pressure ratio p_{x1}/p_{x2}, which is determined by the temperature of the solar collector and the condenser, the recovery ratio r and the index n of polytropic expansion. These three input parameters determine the geometrical proportions of the system with respect to stroke lengths and angular movement. The results for extreme values of the input parameters likely to occur in practice are given in Table 2. It can be seen that, for a range of steam pressure ratios and recovery ratios, the ratio of stroke lengths $\Delta y/\Delta x$ is close to unity in all cases, while the relative length of the crank $R/\Delta x$ varies between 1.11 and 1.87, with higher pressure ratios and recovery ratios requiring a shorter crank. The initial and final angular positions of the crank are in the range $\theta_1 = 6°$ to 22° and $\theta_2 = 67°$ to 87°. The choice of the value of n makes hardly any difference to the results. This implies that the choice of working fluid (steam, organic, siloxane etc) or its state (wet or superheated) does not affect significantly the geometry of the crank mechanism. Due to the insensitivity to this parameter, n is fixed at $n = 1.3$ throughout the rest of this study.

Table 2
Dimensions and efficiency η_{crank} of the crank arrangement for extreme values of the three design parameters: pressure ratio, p_{x1}/p_{x2}, recovery ratio r and index of polytropic expansion n. The stroke Δy of the pump piston and the radius R of the crank are normalised to the stroke Δx of the power piston. The starting and finishing angles of the crank, θ_1 and θ_2 respectively, correspond to those indicated in Fig. 3.

	$r = 0.5$	$r = 0.9$
(a) $n = 1.135$ (saturated steam)		
$p_{x1}/p_{x2} = 3$	$\Delta y/\Delta x = 1.04$ $R/\Delta x = 1.87$ $\theta_1 = 21°$ $\theta_2 = 67°$ $\eta_{crank} = 0.94$	$\Delta y/\Delta x = 0.91$ $R/\Delta x = 1.20$ $\theta_1 = 14°$ $\theta_2 = 82°$ $\eta_{crank} = 0.75$
$p_{x1}/p_{x2} = 10$	$\Delta y/\Delta x = 1.11$ $R/\Delta x = 1.41$ $\theta_1 = 10°$ $\theta_2 = 74°$ $\eta_{crank} = 0.80$	$\Delta y/\Delta x = 0.99$ $R/\Delta x = 1.11$ $\theta_1 = 6°$ $\theta_2 = 85°$ $\eta_{crank} = 0.56$
(b) $n = 1.3$ (superheated steam)		
$p_{x1}/p_{x2} = 3$	$\Delta y/\Delta x = 1.02$ $R/\Delta x = 1.84$ $\theta_1 = 22°$ $\theta_2 = 67°$ $\eta_{crank} = 0.94$	$\Delta y/\Delta x = 0.90$ $R/\Delta x = 1.20$ $\theta_1 = 14°$ $\theta_2 = 82°$ $\eta_{crank} = 0.75$
$p_{x1}/p_{x2} = 10$	$\Delta y/\Delta x = 1.07$ $R/\Delta x = 1.38$ $\theta_1 = 11°$ $\theta_2 = 75°$ $\eta_{crank} = 0.79$	$\Delta y/\Delta x = 0.98$ $R/\Delta x = 1.11$ $\theta_1 = 6°$ $\theta_2 = 85°$ $\eta_{crank} = 0.55$

As noted, the crank mechanism provides a circular motion which is intended to approximate Eq. (6) but does so imperfectly. Fig. 4 compares the provided and ideal motions for differing values of the

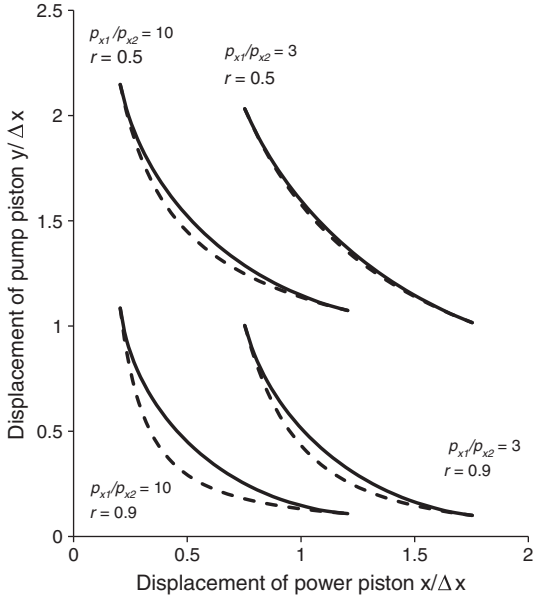

Fig. 4. Circular trajectories of the point P provided by the crank mechanism (solid lines) compared to ideal trajectories based on Eq. (6) (dashed lines), for differing values of working fluid pressure ratio p_{x1}/p_{x2} and recovery ratio r. In all cases $n = 1.3$. Displacements are normalised to the stroke Δx of the power piston. In each case the crank is dimensioned and positioned so that the two curves meet and have equal slope (resulting in equal mechanical advantage) at each of their end points.

input parameters. The greatest deviation occurs at high pressure ratios and recovery ratios. Such deviation results in a loss of energy by the system, because the mechanical advantage will, at some positions of the crank, be less than that required to drive the pump piston. Consequently the power piston will need to be oversized proportionately, resulting in an excess use of working fluid and input energy. The associated efficiency of the crank η_{crank} is given by:

$$\eta_{crank} = \frac{\text{Mechanical advantage provided}}{\text{Mechanical advantage required}} \tag{14}$$

where the mechanical advantage provided is found from Eq. (4), while the mechanical advantage required is calculated as follows:

$$\text{Mechanical advantage required} = \frac{F_y}{F_x} = \frac{\left(p_y / p_{y1}\right)}{\left(p_x / p_{x1}\right)} \frac{p_{y1} A_y}{p_{x1} A_x} \tag{15}$$

Using the relations provided in Appendix A, Eq. (15) becomes

$$\text{Mechanical advantage required} = \frac{\left(y/y_1\right)^{-1}}{\left(x/x_1\right)^{-n}} \frac{1}{\beta\left(\frac{\Delta y}{\Delta x}\right)} \tag{16}$$

where the values of y/y_1 and x/x_1 are calculated based on the circular movement of the point P at the end of the crank. The efficiency in Eq. (14) varies over the motion of the crank, and the value used is the lowest one (ie. worst case) since this will determine the sizing of the piston needed to maintain adequate force. In practice this occurs just before the crank has reached its final position. Fig. 5 shows the results of the calculation of η_{crank} as a function of pressure ratio for three different values of recovery ratio. This shows that higher pressure and recovery ratios give rise to lower efficiencies, as anticipated from Fig. 4. At high pressure ratios it becomes desirable to expand the vapour in more than one stage, such that multiple pistons driving the crank mechanism.

4.2. The RO process

The RO process will not achieve ideal efficiency because real RO processes operate at pressures above the osmotic pressure of the bulk solution. The excess pressure, which corresponds to an energy loss, is required: (i) to provide a net driving pressure to overcome hydraulic resistance to water flowing through the membrane and (ii) to compensate for concentration polarisation whereby solute molecules are swept towards the membrane by the permeate flux, leading to a locally higher osmotic pressure. Thus the total pressure will be:

$$p_y = cp_{osm} + \frac{J}{S} \tag{17}$$

where the concentration polarisation module C represents the concentration of salts near the surface of the membrane divided by that in the bulk solution, J is the flux of water through the membrane and S is its permeability.

The minimum flux that must be used depends on the purity required in the permeate, since smaller flux tends to lead to a more saline permeate [13]. Thus the flux needed to obtain a required level of purity can be calculated from the salt transport coefficient B of the membrane as:

$$J = BC\frac{p_{osm}}{p_{osmp}} \tag{18}$$

where p_{osmp} is the maximum pressure allowable in the permeate (which depends only on the allowable salinity in the permeate).

Substitution of Eq. (18) into Eq. (17) gives the ratio of the total pressure needed over the ideal minimum pressure for the process (ie. the osmotic pressure).

$$\frac{p_y}{p_{osm}} = C\left[1 + \frac{B}{Sp_{osmp}}\right] \tag{19}$$

The foregoing ratio is the overpressure ratio k referred to earlier. It is essentially the inverse of the efficiency η_{RO} of the RO process and Eq. (19) shows that it is independent of the feed salinity. However, there is a third loss to take into account which is the energy needed to drive the recirculation pump. The recirculation flow will determine the recovery factor r_{circ} in the recirculation loop, which will be less than the system recovery ratio r since the permeate has several chances of being recovered in this loop. It is necessary to maintain a sufficiently high r_{circ} to moderate the concentration polarisation C and maintain almost constant concentration along the length of the channel. Here we assume the following relation for C based on fully developed flow [14]:

$$C = 1 + \frac{J^2 b^2}{6D^2} r_{circ} \tag{20}$$

where D is the diffusivity of the salt and b is the channel height. It is assumed in this analysis that C is maintained at ≤ 1.1; thus the maximum allowable value of r_{circ} is obtained from Eq. (20). The actual value adopted was the smaller of this value and 0.1. For such small values of r_{circ}, the cross flow Q_{circ} in the module is worked out from the permeate flow JA:

$$Q_{circ} = \frac{JA}{r_{circ}} \tag{21}$$

Then the pressure drop along the filtration channel is calculated based on the model of laminar flow between two flat plates (this is a reasonable approximation for a spiral wound membrane because the radius of curvature is large compared to the channel height b). Therefore:

$$p_{circ} = Q_{circ}\frac{12\mu l}{bw^3} \tag{22}$$

where μ is the viscosity of the solution, l is the channel length in the direction of flow and w is the width [15]. Note that it is assumed that

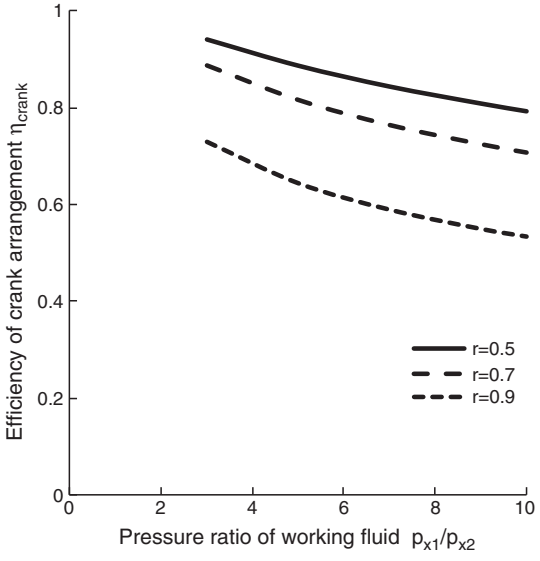

Fig. 5. The efficiency η_{crank} of coupling between the power piston and the pump piston, taking into account deviations of the circular motion of the crank from the ideal motion required to match forces and displacement between the two pistons. The graph shows that η_{crank} decreases with increasing pressure ratio and with increasing recovery ratio r. ($n = 1.3$).

Table 3
Characteristics of the RO membrane module assumed in this study.

Type		BW-2540 spiral wound (Dow Filmtec)
Area A	m^2	2.40
Length l	m	0.95
Width w	m	2.53
Channel height b	m	0.071
Permeability S	$ms^{-1}\,Pa^{-1}$	8.0×10^{-12}
Salt transport coefficient B	ms^{-1}	1.8×10^{-7}

Q_{circ} is approximately constant along the length of the channel, which is justified by the fact that r_{circ} is in practice small. Thus the parasitic power of recirculation is calculated by multiplying p_{circ} by Q_{circ} and dividing by a pump efficiency taken as 0.5. This additional energy is taken into account in the final calculation of η_{RO}, based on the assumption that the energy to drive the recirculation pump will be extracted from the moving crank.

In practical terms RO membrane modules are available with very specific dimensions which are mostly standardised across the industry. Example results will be given for a representative membrane module (whose characteristics are shown in Table 3) typically used for brackish water and whose properties are well characterised. It is assumed that this will be used with sodium chloride solution at 20 °C. The main parameters that can be varied are the feed concentration, allowable permeate concentration and recovery ratio (osmotic pressure is assumed to be proportional to concentration). The allowable permeate concentration is set here at 500 ppm. Values of $B=1.8\times10^{-7}$ ms^{-1} and $S=8.0\times10^{-12}$ ms^{-1} Pa^{-1} are taken from the experimental study of reference [16] . With these parameters fixed, Fig. 6 shows the effect on η_{RO} of varying the recovery ratio r between 0.5 and 0.9 and the feed salinity between for feed salinities in the range 2000 to 14000 ppm. It can be seen that the efficiency has a value of 0.58 at low values of feed concentration and recovery, but decreases sharply for high values. This is due to the increased power requirement of the recirculation flow needed to overcome concentration polarisation.

5. System Examples

Based on the foregoing analysis, it is now possible to provide examples of the expected performance of the whole system in terms of water output per land area of collector used. The examples given are based on two standard solar collector technologies: (i) the parabolic trough collector (PTC) using evacuated tubes which is assumed to provide collection efficiencies of 60% and (ii) the linear Fresnel reflector (LFR) using insulated receiver tubes, providing 35% collection efficiency. The first of these is the most established technology for thermal solar energy conversion; the second a well-known but so far less established technology that could offer lower cost and that has the advantage of a fixed receiver which facilitates direct steam generation [17]. The conditions of the steam provided by these systems are assumed to be 20 bar at 250 °C (PTC) and 15.5 bar at 200 °C (LFR). The condenser is assumed to operate at 40 °C and 0.1 bar, or alternatively at 100 °C and atmospheric pressure.

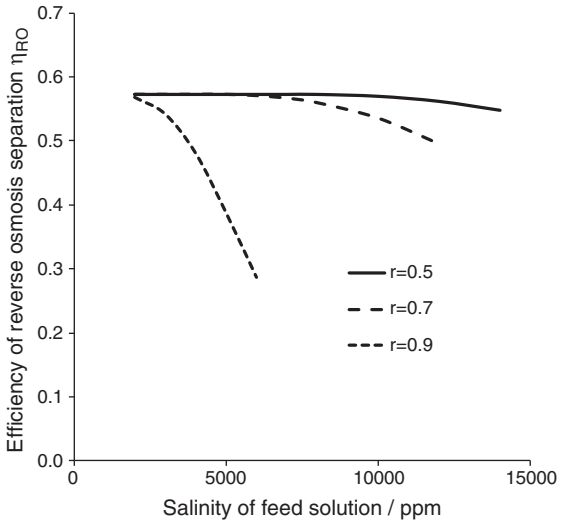

Fig. 6. The efficiency of the reverse osmosis separation, taking into account losses due to the finite permeability of the membrane, concentration polarisation and the need to supply extra power for the recirculation pump. Results are shown for three different values of the recovery rate r. Efficiency deteriorates with increasing feed salinity and with increasing r.

From these values, the ideal Rankine cycle efficiency is calculated by standard procedure with the help of steam tables. Though the expansion of the working fluid is assumed to be isentropic in Eq. (2), in reality losses and irreversibilities will occur in the Rankine cycle and these are taken into account by including an isentropic efficiency of 0.75 in the calculation of the Rankine cycle efficiency η_{rank}.

The calculation of the overall efficiency of solar conversion into the free energy of desalinated components is then given by:

$$\eta = \eta_{coll}\eta_{rank}\eta_{crank}\eta_{RO} \tag{23}$$

The specific consumption of solar energy per water output is now obtained from Eq. (1)

$$\frac{E}{V} = \frac{1}{\eta}p_{osmf}\frac{1}{r}ln\frac{1}{(1-r)} \tag{24}$$

This allows the water output to be estimated given the useful solar irradiation available at the aperture of the collectors (for the LFR this aperture is defined as the horizontal plane and therefore the incident solar irradiation is less than for the PTC whose aperture tracks the sun). In converting water output per collector to land area, it is necessary to make an assumption about the spacing of the collectors. To avoid shadowing, the PTC is assumed to be spaced at a pitch of three times the collector aperture width. As shadowing does not apply to the LFR but space is still needed for access and maintenance, the LFR arrays are closed spacer at a pitch of 1.5 times the width of the mirror arrays. Note that the calculation of the area does not include additional space needed to house the RO equipment and ancillary equipment and services.

Following the foregoing method and assumptions, Table 4 presents four examples of system performance with variations in solar collector technology, feed water salinity, and condenser temperature. Specific solar energy consumption is predicted to be in the range 1.8 to 7.5 kWh/m^3 (6.5 to 27 MJ/m^3) and freshwater output per land area is in the range of 350 to 1030 l/m^2.

Table 4
The final results of the study: examples of system performance using the BW-2540 type RO module together with two types of solar collector (parabolic trough collector, PTC, and linear Fresnel reflector, LFR). Maximum permeate salinity of 500 ppm.

Collector type		PTC	PTC	LFR	LFR
Collection efficiency η_{coll}		0.6	0.6	0.35	0.35
Solar irradiation available ($kWh/m^2\cdot day$)		5.5	5.5	4	4
Steam condition at expansion cylinder inlet	bar	20	20	15.5	15.5
	°C	250	250	200	200
Steam condition in condenser	bar	0.1	0.1	0.1	1
	°C	46	46	46	100
Feedwater salinity (ppm)		3000	5000	5000	5000
Recovery ratio r		0.7	0.7	0.7	0.7
Number of expansion stages		3	3	3	2
Collector area/land area		0.33	0.33	0.67	0.33
Specific solar energy consumption (kWh/m^3)		1.8	3.0	5.3	7.5
Water output per land area ($l/m^2.day$)		1030	620	500	350

6. Conclusion

This paper has analysed a new concept for a solar-powered desalination system using the steam Rankine cycle coupled to a RO process. It uses two pistons, one to expand the steam and the other to compress the saline water. The pistons are linked using a crank mechanism that matches the forces between the two pistons. The efficiency η_{crank} of matching provided by the crank mechanism has been analysed and presented in terms of dimensionless variables for maximum generality. It depends on the expansion ratio of the steam and the recovery ratio and decreases as these variables increase, thus η_{crank} is typically in the range 0.55 to 0.94. The efficiency of the batch RO process has also been studied in relation to the feed salinity and recovery ratio.

It is predicted that, with a feed salinity of 5000 ppm, the overall water output of the system can exceed 500 l per day per m^2 of land occupied by the solar collectors which are of sun tracking type to achieve the temperatures necessary for steam generation. This compares favourably with existing PV–RO systems and prior Rankine–RO systems as discussed in the Introduction. (However, those systems used stationary solar collectors making exact comparisons of land area difficult as the results will depend on the assumptions regarding spacing and shadowing among solar collectors). Even if the steam cycle is operated without a vacuum condenser for simplicity, an output of 350 l per day per m^2 is predicted. Thus a solar installation covering 1000 m^2 could produce 350 m^3 or more of desalinated water per day. Recovery ratios of 0.7 or higher are possible with feed salinities up to 10000 ppm.

The system relies on simple solar collector technology such as the Linear Fresnel Reflector which, due to its low cost compared to say PV collectors, could enable an economical system to be developed. Before reliable cost estimates can be made, however, more work will be needed to develop the detailed mechanical design and to verify performance through experiments. Alongside such experimental work, a software simulation model should be developed which will take into account more details of the process, including frictional losses in individual pipes and valves. Such a model will aid with the optimisation of the new desalination system.

Acknowledgements

The author acknowledges funding from the Engineering and Physical Sciences Research Council, grant reference EP/E044360/1.

Appendix A

This appendix gives the derivation of Eq. (7). Suppose $\mathbf{s}_1$ and $\mathbf{s}_2$ are unit tangent vectors to the trajectory of the point P corresponding to Eq. (6) at the beginning and end of the crank motion. Following the assumption that the linkages LP and MP are longer than OP, the vector joining the initial and final positions of P is $(\Delta x, \Delta y)$. For a circle to fit the slope and position of P at both these points:

$$(\mathbf{s}_1 - \mathbf{s}_2)\cdot\ (\Delta x, -\Delta y\ ) = 0 \tag{A.1}$$

Thus

$$(\mathbf{s}_1 - \mathbf{s}_2)\cdot(1,\ -\Delta y / \Delta x\ ) = 0 \tag{A.2}$$

Now the unit tangent vectors can be expressed in terms of the gradient of the trajectory:

$$\mathbf{s}_1 = \frac{\left\{1, \left(\frac{dy}{dx}\right)_1\right\}}{\sqrt{1 + \left(\frac{dy}{dx}\right)_1^2}} \quad \mathbf{S}_s = \frac{\left\{1, \left(\frac{dy}{dx}\right)_2\right\}}{\sqrt{1 + \left(\frac{dy}{dx}\right)_2^2}} \tag{A.3}$$

These gradients can themselves be expressed in terms of the ratios of the forces acting at P. Since the network done at P should be zero,

$$\begin{aligned}\left(\frac{dy}{dx}\right)_1 &= \frac{-F_{x1}}{F_{y1}} \\ &= \frac{-p_{x1}A_x}{p_{y1}A_y} \\ &= \frac{-p_{x1}(V_{x2} - V_{x1}) / \Delta x}{p_{y1}\left(V_{y2} - V_{y1}\right) / \Delta y} \\ &= -\frac{\Delta y}{\Delta x}\frac{p_{x1}V_{x1}\left[\left(\frac{p_{x1}}{p_{x2}}\right)^{1/n} - 1\right]}{p_{y1}V_{y1}r}\end{aligned}$$

Thus using the definition of β already given in Eq. (8),

$$\left(\frac{dy}{dx}\right)_1 = -\frac{\Delta y}{\Delta x}\beta \tag{A.4}$$

A similar procedure yields:

$$\left(\frac{dy}{dx}\right)_2 = -\frac{\Delta y}{\Delta x}\beta\varepsilon \tag{A.5}$$

Substitution of Eqs. (A.4) and (A.5) into (A.3) and thus into (A.2) leads to a polynomial expression, whose solution gives the Eq. (7) as required.

References

[1] G. Singh, Salinity-related desertificatioin and management strategies: Indian experience, Land Degradation and Development 20 (2009) 367–385.
[2] E. Mathioulakis, V. Belessiotis, E. Delyannis, Desalination by using alternative energy: review and state-of-the-art, Desalination 203 (2007) 346–365.
[3] G. Tiwari, A. Tiwari, Solar Distillation Practice for Water Desalination Systems, 2008, Anshan.
[4] A. Ghermandi, R. Messalem, Solar-driven desalination with reverse osmosis: the state of the art, Desalination and Water Treatment 7 (2009) 285–296.
[5] B.S. Richards, A.I. Schäfer, Photovoltaic-powered desalination system for remote Australian communities, Renewable Energy 13 (2003) 2013–2022.
[6] O. Headley, Renewable energy technologies in the Caribbean, Solar Energy 59 (1997) 1–9.
[7] J.J. Libert, A. Maurel, Desalination and renewable energies — a few recent developments, Desalination 39 (1981) 363–372.
[8] L. García-Rodríguez, A.M. Delgado-Torres, Solar-powered Rankine cycles for fresh water production, Desalination 212 (2007) 319–327.
[9] DLR, AQUA-CSP: Concentrating Solar Power for Seawater Desalination, 2007, Stuttgart.
[10] G.F.C. Rogers, Y.R. Mayhew, Engineering Thermodynamics Work and Heat Transfer, Longman, 1992.
[11] I. Karassik, et al., Pump Handbook, 4th ed, McGraw Hill, 2008.
[12] W. Childs, A. Dabiri, US 6470683 controlled direct drive engine, , 2002.
[13] A. Riedinger, C. Hickman, Considerations of energy consumption in desalination by reverse osmosis, Desalination 40 (1982) 259–270.
[14] M. Porter, Membrane filtration, in: P. Shchweitzer (Ed.), Handbook of Separation Techniques for Chemical Engineers, McGraw Hill, 1979.
[15] B. Massey, Mechanics of Fluids, 4 ed, Van Rostrand Reinhold, 1979.
[16] Davies, P.A. and A.K. Hossain, Development of an integrated RO-greenhouse system driven by solar photovoltaic generators. Desalination and Water Treatment, 2010. in press.
[17] J. Nixon, P. Dey, P.A. Davies, Which is the best solar thermal collection technology for electricity generation in north-west India? Evaluation of options using the analytical hierarchy process, Energy 35 (2010) 5230–5240.